J. Plasma Physics (2003), *vol.* 69, *part* 2, *pp.* 109–130. © 2003 Cambridge University Press
DOI: 10.1017/S0022377803002150 Printed in the United Kingdom

Sawtooth characteristics in ohmically heated HT-7 plasma

LIQUN HU, BAONIAN WAN, YUEJIANG SHI, SHENGXIA LIU, BILI LING and YI XU

Institute of Plasma Physics, Chinese Academy of Sciences, PO Box 1126, Hefei 230031, People's Republic of China

(lqhu@mail.ipp.ac.cn)

(Received 10 June 2002 and in revised form 26 August 2002)

Abstract. The sawtooth activity in an ohmically heated plasma on the HT-7 tokamak has been investigated experimentally using soft x-ray (SXR) diode arrays, magnetic probes and other diagnostics. Its behaviour and occurrence are correlated closely to the discharge conditions such as the electron density N_e, the electron temperature T_e, the safety factor q_a on the plasma boundary and the wall condition, etc. Generally speaking, as N_e increases, the sawtooth activity grows, becoming stronger with a longer period T_s, a larger inversion radius r_s and a larger amplitude fluctuation $\Delta I_{sx}/\bar{I}_{sx}$ on the SXR radiation intensity signal, and evolve from a small to a moderate sawtooth, to a large or even a giant sawtooth. Sometimes, a double sawtooth and a monster sawtooth activity emerge without apparent deterioration of the plasma confinement and without major plasma disruption. During the events, abundant magnetohydrodynamic phenomena are observed, including a long partial sawtooth collapse. In this paper, the general sawtooth behaviour and the dependence of the occurrence of the sawtooth instability on the electron density N_e and wall condition have been summarized. Experimental properties of two types of double sawtooth and monster sawtooth activities are also presented and discussed. The set up of the HT-7 tokamak and the main diagnostics available are also briefly described.

1. Introduction

The sawtooth instability, characterized by a periodic collapse of the pressure or internal disruption in the plasma core, belongs to the most typical form of magnetohydrodynamic (MHD) activity. Since sawtooth oscillations were discovered in 1974 [1], they have been widely studied in many tokamaks both experimentally and theoretically [2–10]. The results have continuously stimulated extensive investigation and development in this area of research. Experimental results in many tokamaks have convincingly shown that the sawtooth instability plays a crucial role in the determination on the central plasma heating and confinement, and in the regulation of the core plasma performance. Although it is possible to suppress the sawtooth activity by increasing the central electron temperature $T_e(0)$ and driving the central safety factor $q_0 > 1$ in the reverse shear plasma, the sawtooth activity is still one of the limitations of the central plasma temperature achieved in a tokamak

https://doi.org/10.1017/S0022377803002150 Published online by Cambridge University Press

independent of the input power, while tokamak parameters approach to the ignition condition particularly in large tokamaks such as JET and JT-60U. The study and modification of the sawtooth instability have become more and more important issues.

In the plasma, the intensity I_{sx} of the soft x-ray (SXR) radiation depends on the electron density N_e, the electron temperature T_e and the impurity concentration of the plasma (described by the effective charge Z_{eff}). A variation in either of these quantities will cause a fluctuation of the SXR radiation. Since the SXR radiation signal is very sensitive to the variation of the electron density N_e in proportion to N_e^2, the variation of N_e and its fluctuation $\Delta N_e/N_e$ will bring about relative changes of the amplitude I_{sx} and the overlapped disturbance $\Delta I_{sx}/\bar{I}_{sx}$ on the SXR radiation signal. However, the sawtooth oscillation on the SXR radiation signal is caused predominantly by the fluctuation of the electron temperature T_e.

Most of the radiation received by a given SXR detector comes from the small volume where the temperature and the density have their maximum value along the viewing chord. The chord-integrated measurement of SXR emission is more of a point measurement rather than an averaged one at the peak of the SXR profile, which can be of high spatial resolution and with a high temporal response to the variations occurring inside of the plasma. The analysis of the fluctuation in the intensity of the continuous SXR emission from the discharge has become a standard technique for understanding the observed phenomena related to the plasma instability. The spatial distribution, evolution and tomography of the SXR emission can provide considerable information on the plasma structure, MHD instability, sawtooth collapse instability, phenomena occurring during major disruptions and heat pulse propagation transport, etc.

Various theoretical models have been proposed to explain sawtooth oscillations: ideal MHD convection [5, 6], magnetic reconnection due to resistivity [7] and due to electron inertia [8], enhanced cross-field transport [9, 10], etc. Among them, Kadomtsev's magnetic reconnection model [7] is widely accepted at present and can successfully explain the observed phenomena of sawtooth instability in small tokamaks, where a growing island caused by the $m = 1$ tearing mode instability replacing a shrinking hot core resulting in the sawtooth collapse. However, for large tokamaks such as JET, the predictions of Kadomtsev's model have many deviations from some of the observed phenomena [11, 12], such as much shorter time to the sawtooth collapse and no precursor oscillations preceding the collapse of the compound sawtooth, etc. To solve these disagreements, many models were proposed including Wesson's quasi-interchange mode [6], where he suggested a convective flow between a crescent hot core and a colder bubble resulting in sawtooth collapse owing to the $m = 1$ ideal mode instability.

In the HT-7 tokamak device, the sawtooth activity and other observed phenomena related to the plasma instability have been investigated experimentally using two SXR multi-channel diode arrays, magnetic pick-up probes and other diagnostics. In this paper, the general sawtooth behaviour and the dependence of the occurrence of the sawtooth instability on the electron density N_e and the wall condition has been summarized. Experimental properties of two types of double sawtooth and monster sawtooth activities are also presented and discussed. During the events, abundant MHD phenomena including a long partial sawtooth collapse are exhibited.

https://doi.org/10.1017/S0022377803002150 Published online by Cambridge University Press

2. HT-7 device experimental set-up [13, 14]

The HT-7 device, reconstructed from the original Russian T-7 tokamak in 1994, is a medium-sized superconducting tokamak with a major radius of $R = 1.22\,\mathrm{m}$ and a minor radius of $a = 0.3\,\mathrm{m}$ in the circular cross-section. Its major research fields focus on the exploration of advanced steady-state operation, high-performance plasma discharge and a plasma fuelling study, including LHCD, LHW and ICRF heating. The HT-7 tokamak has a stainless-steel liner with a radius of 0.32 m, two fixed and two movable stainless-steel limiters with molybdenum tips. Its ohmic heating transform has an iron core and can offer a magnetic flux of up to 1.8 V S. 24 superconducting coils located between two layers of thick copper shells produce and maintain the toroidal magnetic field B_t ($\leqslant 2.5\,\mathrm{T}$). From the spring experimental campaign in 1998, a feedback control system has been developed and successfully put into routine operation to simultaneously control the plasma current, plasma density and plasma displacement. The HT-7 machine operates normally at the following parameters: plasma current $I_p = 100$–$250\,\mathrm{kA}$ with a duration of 3–5 s, central chord-averaged electron density $\bar{N}_e(0) = 0.8$–$5.0 \times 10^{13}\,\mathrm{cm}^{-3}$, central electron and ion temperatures $T_e(0) = 0.5$–$1.0\,\mathrm{keV}$ and $T_i(0) = 0.5\,\mathrm{keV}$, energy confinement time $\tau_E = 15\,\mathrm{ms}$ and effective charge $Z_{\mathrm{eff}} = 2$–3.

The main diagnostics available on the HT-7 device are introduced as follows, some of which are still under development. The electron density profile is measured using a vertical five-channel far-infrared hydrogen cyanide (FIR-HCN) laser interferometer. The electron temperature profile is determined by an ECE radiometer measurement [15] and a multi-point neodymium Thomson scattering with up to five spatial points and eight time points. A three-channel soft x-ray spectrum analyser is applied to measure the central absolute electron temperature. A neutral particle analyser (NPA) collimated to the central channel is used to measure the central ion temperature. The flux distribution of the neutral Hα optical radiation is provided by three multi-channel arrays located at different toroidal positions including an inclined array collimated to the lower half of the high field of the plasma column, and two vertical arrays collimated to the limiter region and the plasma, respectively. A vertical 16-channel XUV bolometer is also used for monitoring the plasma radiation loss. Optical spectra of several major impurities including carbon, oxygen and molybdenum are monitored by line-emission measurements of a four-channel visible bremsstrahlung, a 10-channel C^{3+} and a few single-channel visible lights, etc. Three groups of magnetic pick-up probes located at different toroidal positions, each with 12 probes, allows the analysis of the Mirnov oscillation and mode structure by their azimuthal variations of the magnetic fluctuation in probe signals. There are also many basic diagnostics, including electromagnetic measurement and diamagnetic measurement, etc.

Measurement of x-ray radiation intensity comprises an SXR diagnostic, a seven-channel hard x-ray array and a single horizontal independent hard x-ray detector collimated to the limiter with a NaI scintillator and an energy spectrum analyser. The SXR diagnostic system shown in Fig. 1 consists of a horizontal and a vertical imaging camera with slot-aperture beryllium windows orientated in the toroidal direction [16], which is in fashion similar to that of a pinhole camera. Each camera uses 37 rectangular detectors (Au–Si surface-barrier diode, SBD) housed in a separated stainless-steel vessel. All detectors, each with an active area of $3 \times 20\,\mathrm{mm}^2$ and an energy sensitivity of between 0.3 and 15 keV, are mounted in

https://doi.org/10.1017/S0022377803002150 Published online by Cambridge University Press

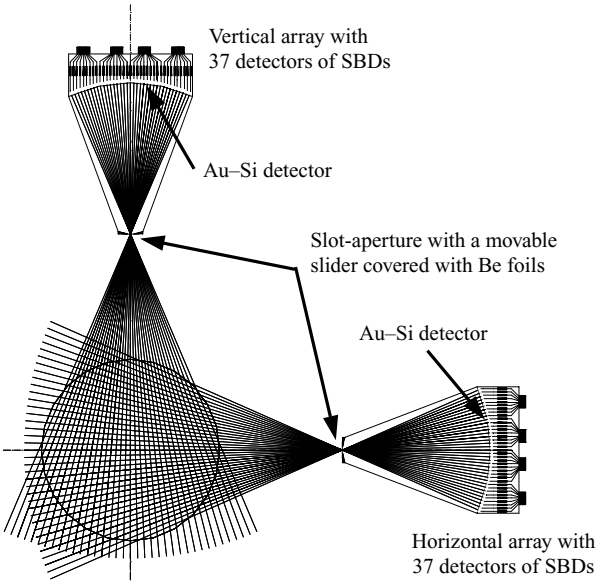


Figure 1. Schematic arrangement of the soft x-ray diagnostic system with SBDs on the HT-7 tokamak device.

an arc-shaped stainless-steel pedestal with $R = 55$ cm in the horizontal array and $R = 60$ cm in the vertical array. Their spatial resolution, the radial distance between neighbouring viewing chords of the detectors, is 1.5 cm. They view a given toroidal cross-section of the plasma from different poloidal angles (from -27 to 27 cm at tangent radii horizontally and vertically) through a thin beryllium window of area $5 \times 20\,\mathrm{mm}^2$ in the vertical array and $4 \times 25\,\mathrm{mm}^2$ in the horizontal array. To satisfy the requirement of different discharge conditions under the available limited space, different mechanics of the changeable beryllium foil are adopted for both cameras to support four foils of different thickness: 5–6, 12–13, 25 μm and full open. To obtain a satisfactory signal-to-noise level, a mechanical structure with multi-metal shields and isolation is applied to screen the detectors from electronic and magnetic field perturbation from the outside.

3. General sawtooth features in an ohmically heated plasma

In the ohmically heated HT-7 plasma, four types of MHD phenomena have been observed with respect to the different SXR fluctuation signal in the central region of the plasma: sinusoid-like Mirnov oscillations, typical sawtooth oscillations, sawtooth-like oscillations and MHD-free. Several types of sawtooth activities have also been identified: small sawtooth, moderate sawtooth, giant sawtooth, double sawtooth and monster sawtooth. They correspond to different internal mode features and their occurrences are correlated closely to the discharge conditions, such as the electron density N_e, the electron temperature T_e, the impurity content Z_{eff} and the edge parameters (the safety factor q_a at the plasma boundary and the wall condition). Sometimes different types of MHD activities and the transitions among them following the fluctuation of plasma parameters in one shot can be observed, as shown in Fig. 2. Along a constant q_a^{-1} line in a Hugill plot, different

https://doi.org/10.1017/S0022377803002150 Published online by Cambridge University Press

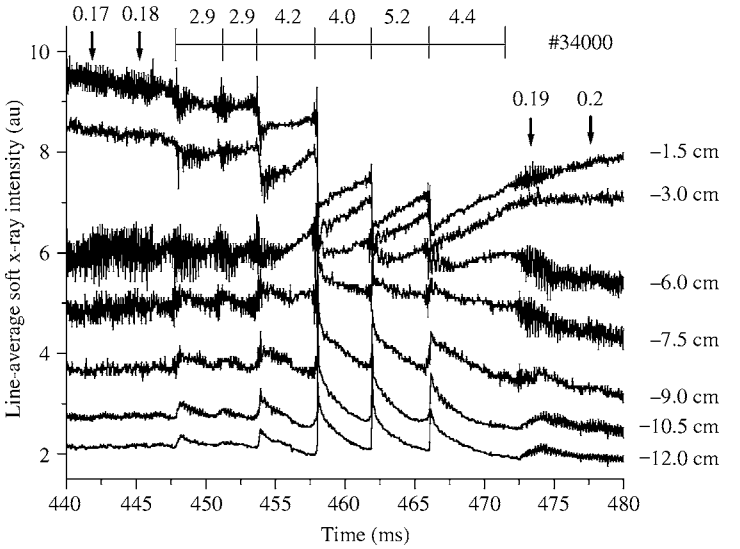


Figure 2. Sawtooth oscillations ($T_{st} = 2.9$–5.2 ms), Mirnov oscillations ($T = 0.17$–0.2 ms) and their transitions on the SXR intensity signal for the typical ohmic shot 34000 ($I_p = 106.9$ kA/0.55 s, $\bar{N}_e(0) = 1.4$–1.7×10^{13} cm^{-3} and $q_a = 4.8$). Note that the relative amplitude is not to scale. Each trace is enlarged individually so that the peak-to-peak amplitude occupies the entire frame.

MHD activities are passed: MHD mode-free, MHD mode generating, mode growing, mode saturating, mode lock and hard disruption. The rotation frequency of MHD modes changes with one shot or different shots [17].

In general, the internal sawtooth collapse in the plasma behaves with two successive phenomena, a precursor oscillation due to plasma rotation and a relaxation of the pressure profile. The precursor oscillation distinctly exhibits an $m = 1/n = 1$ poloidal and toroidal mode structure with a relatively high frequency and a rapidly growing oscillation preceding the sawtooth collapse on the SXR intensity signal. A typical feature of the sawtooth oscillation, as shown in Figs 2 and 3, is that the sawtooth in the central plasma region is positive with a slow rise and then a fast fall, where the relative amplitude fluctuation $\Delta I_{sx}/\bar{I}_{sx}$ on the SXR intensity signal has the largest value. Correspondingly, in the outer region some distance away from the magnetic axis, the sawtooth is reversed with a fast rise and then a slow exponential drop. The radius of the intermediate region is that of a $q = 1$ magnetic surface, called the inversion radius r_s. From the evolution of the sawtooth oscillation, it can be seen that plasma energy is rapidly lost from the central region and transported to outside this region, accompanied by heat and particle transport, which is characterized by progressively delayed and broadened propagation traces of pulse-like sawtooth peaks. The strength or driving force of the sawtooth significantly affects the propagation of the heat pulse perturbation and the behaviour of the gross plasma. The electron heat diffusivity χ_e can be estimated from the heat pulse propagation [18].

Four distinct types of sawtooth collapse during ohmic discharges even for one shot can be seen. First, during the current rise phase, the sawtooth is generally proceeded by the precursor oscillation with rapidly growing amplitude, sometimes the sawtooth inversion radius may be small (only $0.11a$); however, without the

https://doi.org/10.1017/S0022377803002150 Published online by Cambridge University Press

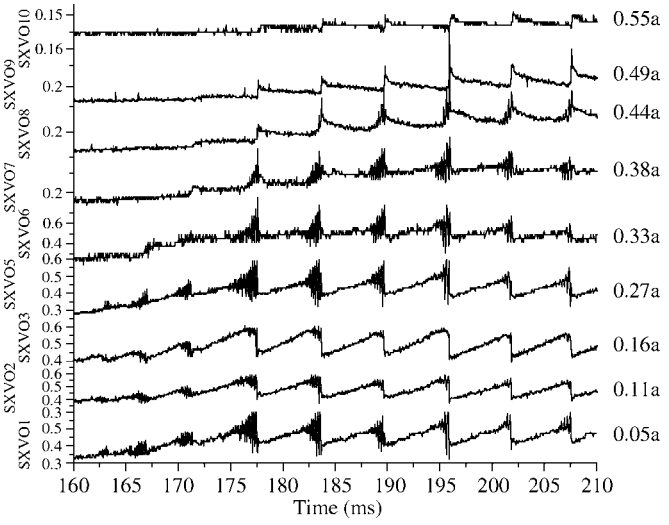


Figure 3. Precursor oscillations preceding the sawtooth collapse during the current rise phase.

obvious successor oscillation as shown in Fig. 3, in which the temperature profile is very peaked. In Fig. 3, the precursor has a high characteristic frequency of 4–9 kHz, its growth time increases gradually from 0.5 to 3.0 ms prior to 178 ms and then decreases to 1.0 ms, however, during the period, the oscillation frequency gradually decreases on successive sawteeth until the end of the precursor at 214 ms. It is consistent with the prediction of the Kadomtsev model. Secondly, during the current flattop in most ohmic discharges, the sawtooth behaviour varies with a single, double and monster sawtooth. Thirdly, successor oscillations are often observed, however, the precursor oscillations are invariably absent. The possible reasons for the absence of precursor oscillation are that the magnetic island possibly does not exist, or the island exists but is locked, or the island exists only with an insignificant rotating or a very small growing time, which is beyond the resolution of the diagnostic instrumentation. Fourthly, both precursor and successor oscillations are observed as in the case of the monster sawtooth, which indicated that the sawtooth collapse does not destroy the magnetic island and does not stop the rotation of the magnetic island.

3.1. Dependence of sawtooth features on the electron density

In the start-up phase of the plasma discharge, plasma parameters vary very quickly, the induced phenomena are very plentiful but complicated, and are difficult to analyse. In general, when the central-line averaged electron density $\bar{N}_e(0)$ is over $0.6 \times 10^{13}\,\mathrm{cm}^{-3}$, the sawtooth oscillation with the precursor activity on the SXR intensity signal emerges.

In the flattop phase of the plasma current, when $\bar{N}_e(0)$ is less than $0.8\times10^{13}\,\mathrm{cm}^{-3}$, the SXR radiation intensity is relatively weak, sometimes the sawtooth-like oscillation emerges with a period of less than 1.0 ms. If $\bar{N}_e(0)$ is too low (less than $0.4\times10^{13}\,\mathrm{cm}^{-3}$), collisions between electrons are reduced and many electrons will be accelerated to high energies. Some of them are not confined and the hard x-ray radiation is strengthened enormously during the whole discharge. For a lower electron

https://doi.org/10.1017/S0022377803002150 Published online by Cambridge University Press

density $\bar{N}_e(0)$ of less than $0.1 \times 10^{13}\,\mathrm{cm}^{-3}$, a great number of energetic electrons will drift outside to bombard the limiter or the vacuum wall, thus producing thick-target bremsstrahlung hard x-rays. The hard x-ray radiation will be violent with many bursts corresponding to the positive spikes occurring on the SXR radiation signal, plasma current and loop voltage.

However, during the current flattop phase of the plasma discharge, when the plasma current I_p is over 120 kA and $\bar{N}_e(0)$ is more than $1.0 \times 10^{13}\,\mathrm{cm}^{-3}$, the sawtooth oscillation on the SXR intensity signal emerges easily. In some cases such as at the peaking distribution of the electron density, the sawtooth oscillation occurs at a lower density threshold of $\bar{N}_e(0) \geqslant 0.75 \times 10^{13}\,\mathrm{cm}^{-3}$. In the range of $\bar{N}_e(0) = 1.0$–$1.5 \times 10^{13}\,\mathrm{cm}^{-3}$, the typical period T_s of the small sawtooth is 0.8–2.5 ms with $\Delta I_{sx}/\bar{I}_{sx} \leqslant 10\%$. In the range of $\bar{N}_e(0) = 1.5$–2.0×10^{13}, the moderate sawtooth activity emerges with T_s up to 4.5 ms and central $\Delta I_{sx}/\bar{I}_{sx} = 10$–$20\%$. When $\bar{N}_e(0)$ is over $2.0 \times 10^{13}\,\mathrm{cm}^{-3}$, the major sawtooth activity appears with T_s up to 6.5 ms and central $\Delta I_{sx}/\bar{I}_{sx} = 20$–$30\%$. When $\bar{N}_e(0)$ is over $2.2 \times 10^{13}\,\mathrm{cm}^{-3}$, sometimes the giant sawtooth activity has a period T_s up to 9 ms and $\Delta I_{sx}/\bar{I}_{sx} = 30$–$40\%$. In the range of $\bar{N}_e(0) = 1.5$–$2.5 \times 10^{13}\,\mathrm{cm}^{-3}$, sometimes the monster sawtooth activity has a period T_s of up to 33.5 ms and core amplitude fluctuations $\Delta I_{sx}/\bar{I}_{sx}$ of up to 76% occur. Although growing MHD oscillations are often visible in the range of $\bar{N}_e(0) = 1.0$–$2.5 \times 10^{13}\,\mathrm{cm}^{-3}$, plasma discharges with the sawtooth oscillation are usually stable without major disruption and can be maintained until the exhaustion of the ohmic heating field.

As the density $\bar{N}_e(0)$ further increases above $2.5 \times 10^{13}\,\mathrm{cm}^{-3}$, the $m = 1/n = 1$ precursor and successor fluctuations overlapped on the sawtooth grow gradually, the sawtooth oscillation may reduce and transit to the sinusoid-like Mirnov oscillation with a high frequency of $f = 4$–9 kHz. These global fluctuations are more intense in the vicinity of a $q = 1$ surface and correspond to Mirnov oscillations on magnetic pick-up probes very well. Sometimes these MHD oscillations may cause plasma disruption, especially at a low-q condition. When $\bar{N}_e$ is high enough to approach the density limit, the plasma will be easily destroyed by a disruptive instability.

3.2. Dependence of sawtooth features on the wall condition [19]

Plasma discharges with the sawtooth oscillation are closely related to the wall condition. In the very clean plasma just after wall conditioning with ICRF boronization, the plasma performance is improved immediately with a significant decrease of radiation power from 50–90% to 10–18% of the ohmic power with the same plasma current condition and density. Recycling is out of control for the first tens of shots and then becomes controllable, with the Z_{eff} dropping close to 2 at $\bar{N}_e(0) = 1.5 \times 10^{13}\,\mathrm{cm}^{-3}$ and 1 at a higher $\bar{N}_e(0) = 5.0 \times 10^{13}\,\mathrm{cm}^{-3}$. During the first 30 shots after ICRF wall boronization, since the electron temperature is very low due to a high wall recycling, the SXR intensity signal is very weak (only around one-tenth of that under the same plasma condition). Plasma discharges are sawtooth-free even at high electron density, reaching the Greenwald density limit (5–$6 \times 10^{13}\,\mathrm{cm}^{-3}$). After the first 30 shots, as the radiation power gradually goes back to the normal level, the SXR radiation increases and recovers gradually, and moderate and major sawtooth oscillations appear in a high electron density of $\bar{N}_e(0) = 1.5$–$2.5 \times 10^{13}\,\mathrm{cm}^{-3}$.

https://doi.org/10.1017/S0022377803002150 Published online by Cambridge University Press

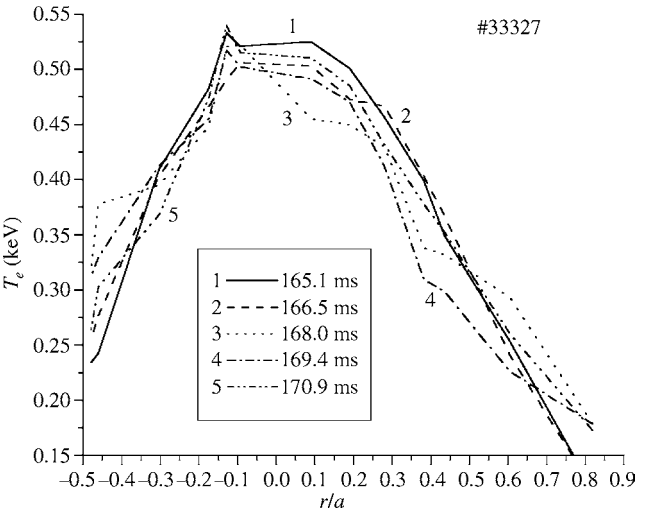


Figure 4. Temporal evolution of the measured electron temperature $T_e(r)$ by an ECE radiometer diagnostic before, during and after a moderate sawtooth collapse at $t = 167.8$ ms for the typical ohmic shot 33327 ($I_p = 130.9$ kA/0.7 s, $\bar{N}_e(0) = 1.5$–2.5×10^{13} cm^{-3} and $q_a = 4.2$).

Wall conditioning with ICRF siliconization is quite different, the radiation power is also reduced but only to one-third of that with RF boronization. After ICRF siliconization, the recycling can be handled easily and the plasma performance improves immediately with a higher plasma current. The plasma can be operated at a low q_a of around 2.45, a wider stable region and a higher electron temperature T_e with the same conditions for the plasma current and density. The major and giant sawtooth oscillations are often observed even for the first shot after ICRF siliconization.

3.3. Variation of the electron temperature during the sawtooth collapse

The electron temperature T_e is very sensitive to the sawtooth collapse and has notable variations during the collapse. For small sawtooth collapses, temporal variations of the electron temperature $T_e(r)$ are too small to be observed due to given time and spatial resolution limitations of the ECE radiometer measurement. For the intense sawtooth collapse, the deep core temperature decreases and even global decreases ($\leqslant 0.6a$) can be observed. The temporal evolution of the electron temperature $T_e(r)$ profile during a moderate sawtooth collapse is given in Fig. 4 and agrees with predictions of the Kadomtsev model quite well. After the sawtooth collapse, a peaked profile of electron temperature T_e inside the $q = 1$ surface becomes unstable due to a rapid redistribution of the plasma energy and enhanced transport through the $q = 1$ surface. As a result, the $T_e(r)$ profile decreases and flattens inside the $q = 1$ surface, and in the meanwhile increases slightly just outside the $q = 1$ surface. The decrease recovers slowly and the increase dies off exponentially due to the ohmic heating. The core decrease of the electron temperature T_e is related to the strength of the sawtooth collapse. Evolution of the SXR intensity signal follows the same trace since the macroscopic plasma parameters do not fluctuate considerably. From Fig. 5, an obvious central decrease of the electron temperature can be seen during the period of the MHD activity on the SXR intensity signal and magnetic pick-up probes from 307 to 510 ms.

https://doi.org/10.1017/S0022377803002150 Published online by Cambridge University Press

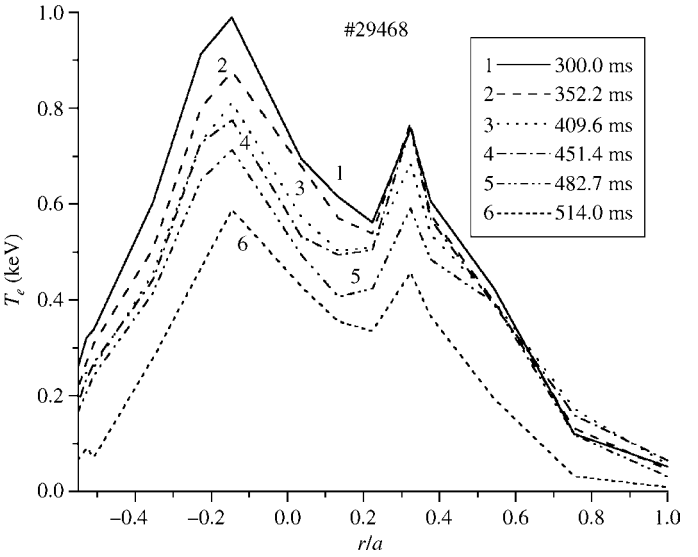


Figure 5. Temporal evolution of the electron temperature $T_e(r)$ by an ECE diagnostic during the period of MHD oscillations on the signals of the SXR intensity and magnetic pickup probes for the typical ohmic shot 29468 ($I_p = 129\,\text{kA}/0.48\,\text{s}$, $\bar{N}_e(0) = 1.4\text{–}1.6 \times 10^{13}\,\text{cm}^{-3}$ and $q_a = 4.1$). A gradual decrease of the electron temperature can be seen clearly after the onset of MHD oscillations at about 307 ms.

4. Double-sawtooth activity in ohmically heated plasma [20, 21]

In the HT-7 tokamak, double-sawtooth activity on the SXR signal occurs occasionally under a low-q condition ($q_a \leqslant 2.8$), especially at high plasma current after the ramp-up phase of the plasma current ($I_p > 190\,\text{kA}$) and/or at medium density (over $2.2 \times 10^{13}\,\text{cm}^{-3}$) after siliconization. It is characterized by two periods and amplitudes per cycle, where the first sawtooth occurs during the rise phase of the central sawtooth. For typical ohmic shot 30988 with the double-sawtooth activity illustrated in Fig. 6, two types of double-sawtooth oscillations are interspersed among single-sawtooth oscillations in an erratic way, as shown in Fig. 7. For the type 1, the sawtooth is slightly doubled with a slightly longer period and a comparable amplitude variation $\Delta I_{sx}/\bar{I}_{sx}$ to that of the single sawtooth. The first sawtooth is a small collapse with a smaller central $\Delta I_{sx}/\bar{I}_{sx}$ than that of the second sawtooth, but takes nearly a whole period; the second sawtooth is usually a 'slow collapse' with a longer collapse time than that of the single sawtooth. For type 2, the sawtooth is remarkably doubled with a period of 1–2 times that of the single sawtooth, and periods of the first sawtooth and the second one are nearly the same. The first sawtooth is also a small collapse and the second sawtooth is often a moderate or major 'fast collapse' with a shorter collapse time and much larger central $\Delta I_{sx}/\bar{I}_{sx}$ than that of the first sawtooth, which can be up to twice that of the single sawtooth. For both types, like most of the single sawtooth, no obvious precursor activities were superimposed on the sawtooth before the first sawtooth collapse and no visible sinusoidal successor activities after the second collapse are found. Only a few single sawteeth have weakly irregular sinusoidal precursors or successors. However, immediately after the first collapse, the successor with a burst of the sinusoidal oscillation appears apparently in the region near an inversion of

https://doi.org/10.1017/S0022377803002150 Published online by Cambridge University Press

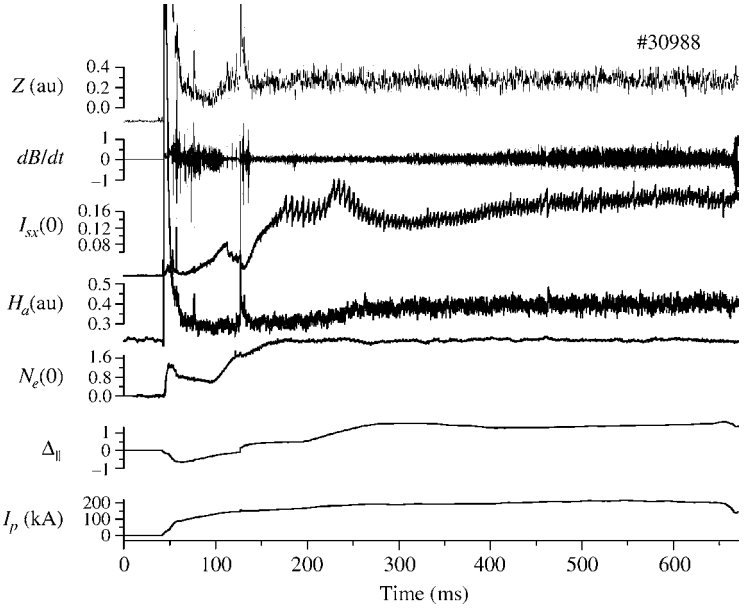


Figure 6. Plasma performance on several diagnostic signals for the typical ohmic shot 30988 with double-sawtooth activity on the SXR intensity signal ($I_p = 216.5\,\mathrm{kA}/0.75\,\mathrm{s}$, $\bar{N}_e(0) = 2.2$–$2.44 \times 10^{13}\,\mathrm{cm}^{-3}$ and $q_a = 2.8$).

radius r_s, almost concurrently with the onset of the collapse, sometimes with the magnitude of the excursion being comparable with the sawtooth amplitude of the SXR intensity signal. These oscillations have a larger perturbation region inside r_s than those outside r_s, sometimes expanding to the centre, which possibly causes the full collapse of the type 1 oscillation. In addition, the inversion radii of the second sawtooth are approximately $\sim$1.5 cm smaller for type 2 and $\leqslant 0.75$ cm smaller for type 1 than those of the first sawtooth within the spatial resolution of the SXR diagnostic. During the whole discharge, the occurrence of type 1 is nearly twice that of type 2, but both much less than that of the single sawtooth. These features suggest that the double-sawtooth activity is not simply a composition of two single-sawtooth oscillations with different periods.

The corresponding relation among the single sawtooth, the double sawtooth and H_α sawtooth can be found in Figs 8(a) and (b). The heat effect on the wall induced by the sawtooth collapse can be clearly seen. It is understood that the plasma energy lost from the central region transports to the outer region in the form of the heat pulse, varying the flux of neutral particles and hence influencing the H_α radiation. The time delay between spikes of the SXR signal and the H_α signal shows the time for heat propagation from centre to edge. It can also be seen that the first collapse of type 2 is of greater strength than that of type 1 but is smaller than that of a single sawtooth and the second collapse of type 2 is of greater strength than that of type 1 and than the single sawtooth collapse. This means only a small amount of heat is released during the first sawtooth to the outside and suggests that the first sawtooth is not a dominant collapse. Except for those during the period of double-sawtooth activity and the transition among the single sawtooth and the two types of double sawtooth, no apparent fluctuations in visible bremsstrahlung Z, impurity

https://doi.org/10.1017/S0022377803002150 Published online by Cambridge University Press

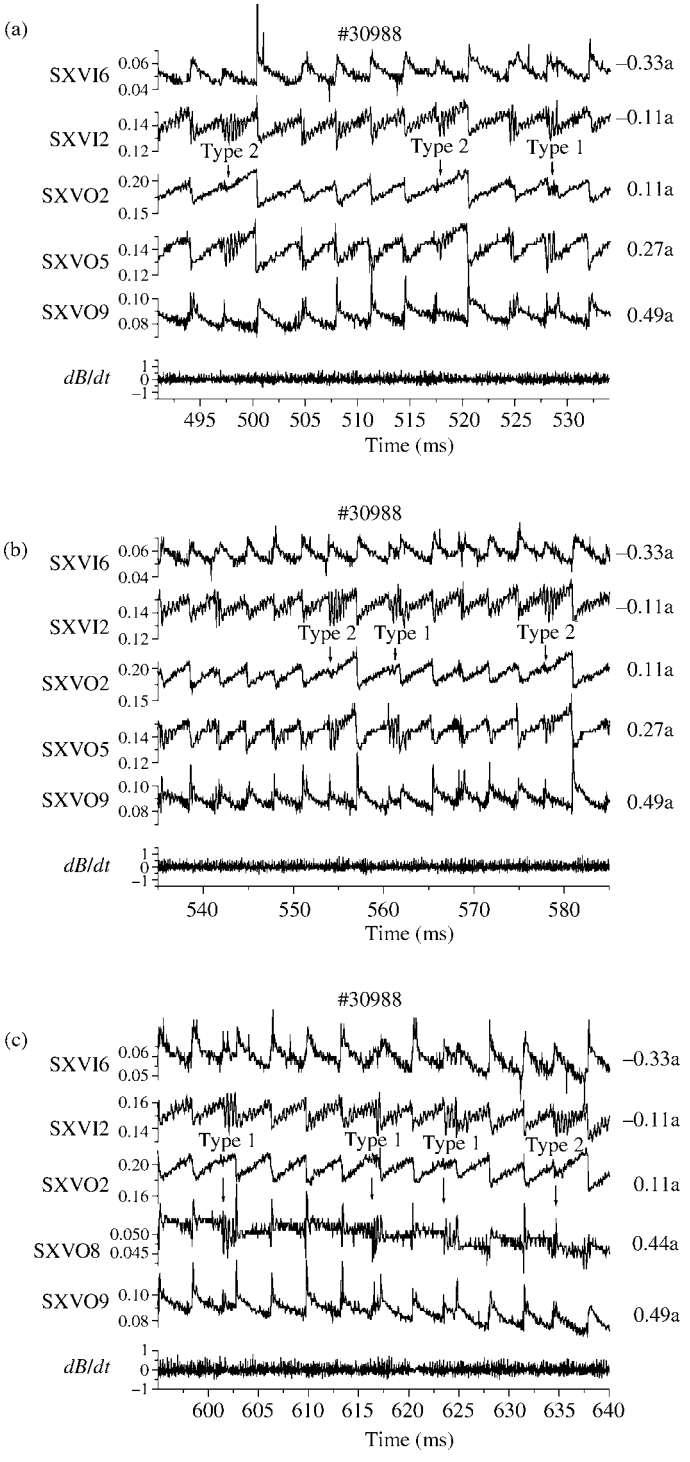


Figure 7. The expanded time traces during different periods (a), (b) and (c) corresponding to Fig. 6 for shot 30988, where two types of double-sawtooth activities (type 1 and type 2) are occasionally interspersed among common single-sawtooth oscillations.

https://doi.org/10.1017/S0022377803002150 Published online by Cambridge University Press

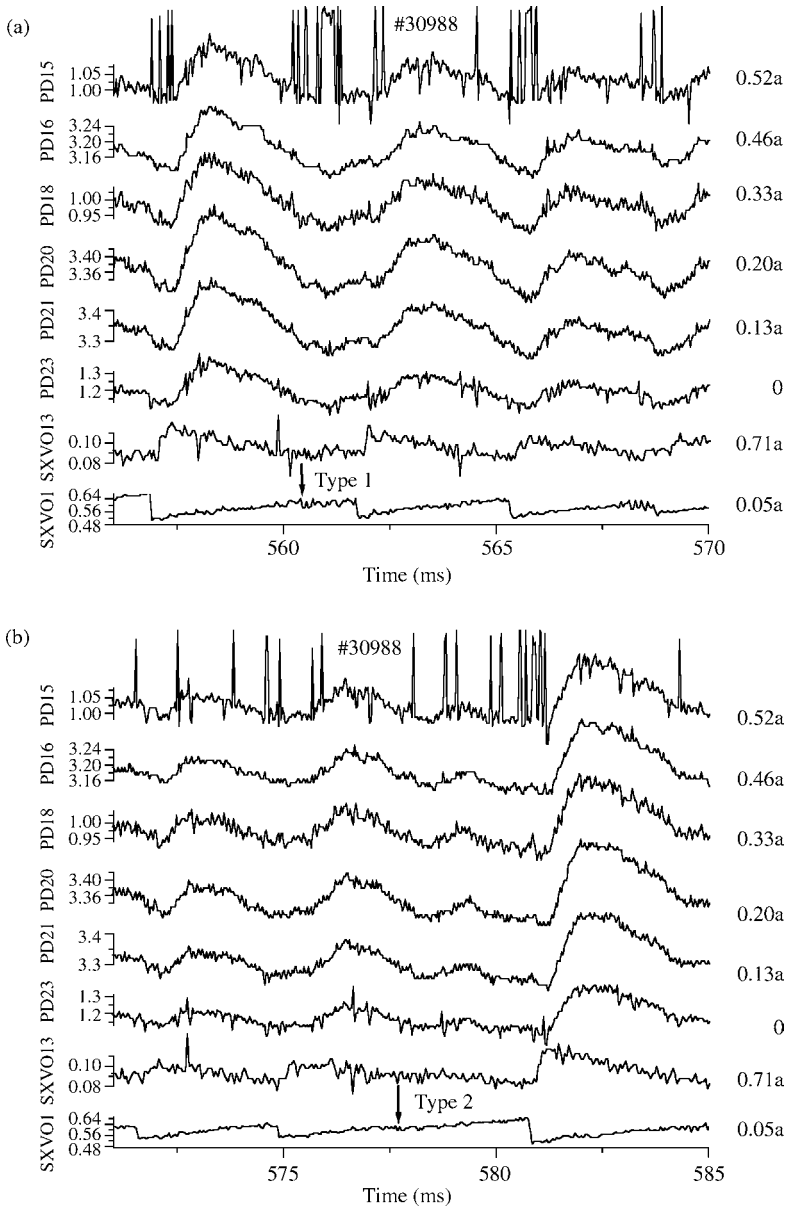


Figure 8. Corresponding relation between the SXR signal and the H_α signal for double sawteeth of type 1 (a) and type 2 (b) including their first collapses. Pd15–Pd23 are the H_α signals collimated to the limit region.

line emissions, XUV bolometer and hard x-ray radiation are found, no observable variations in plasma parameters including the loop voltage and the horizontal displacement $\Delta_\parallel$ (the displacement of the centre of the outermost magnetic surface) and no deterioration of plasma confinement are observed.

For shot 30988, the plasma current ramps up at a low rate of $0.26\,\mathrm{MA\,s^{-1}}$ from 140 to 193.5 ms and at a high rate of $0.4\,\mathrm{MA\,s^{-1}}$ from 193.5 to 258.3 ms. During the

https://doi.org/10.1017/S0022377803002150 Published online by Cambridge University Press

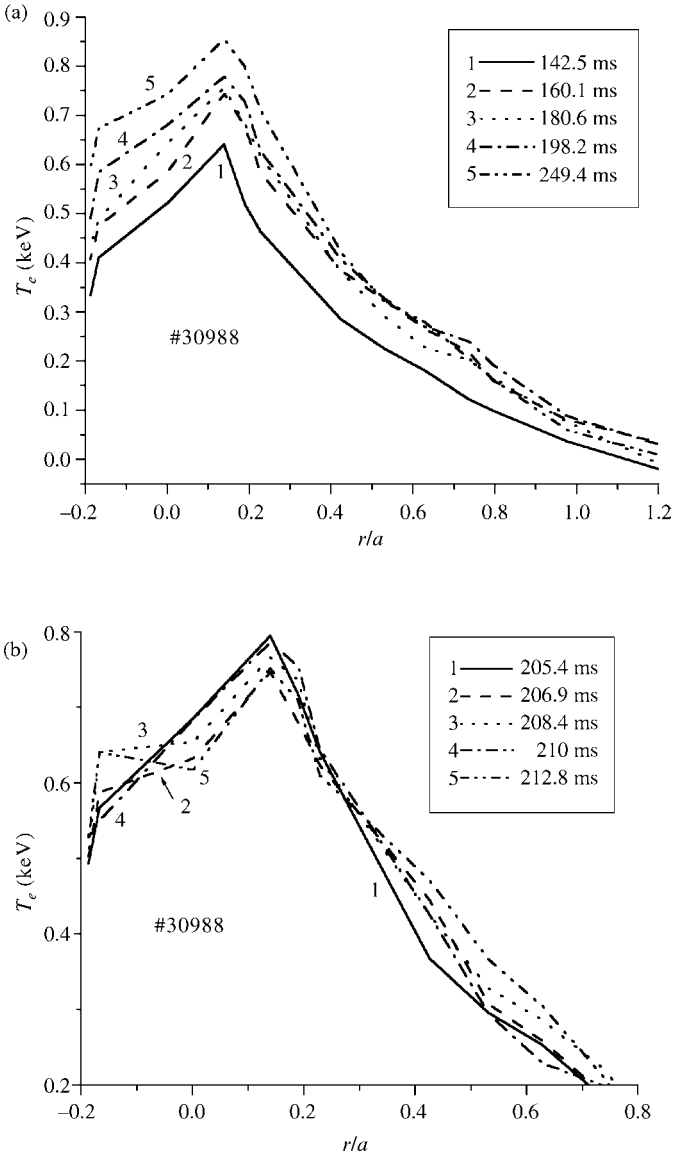


Figure 9. Temporal evolution of the measured electron temperature during a different ramp-up phase of the plasma current for the ohmic shot 30988 with a low rate (a) and a high rate (b) and (c), after the ramp-up phase (d). It can also be seen clearly from Fig. 9(e) that the centroid of the SXR profile shifts to the geometric centre similar to Fig. 9(a).

ramp-up phase, as shown in Fig. 9(a), the electron temperature profile is peaked and continues increasing at the position $0.14a$ of the low-field side (LFS) – obvious effects of ohmic heating can be seen. This is attributed to the effect of current penetration to the core, which is induced by the skin current at the low electron temperature. At the high rate phase, $T_e(-0.17a)$, the temperature at the position $-0.17a$ of the high-field side (HFS), gradually increases but is smaller than $T_e(0.14a)$, the shallowly hollow temperature profile $T_e(r)$ appears intermittantly and then gradually

https://doi.org/10.1017/S0022377803002150 Published online by Cambridge University Press

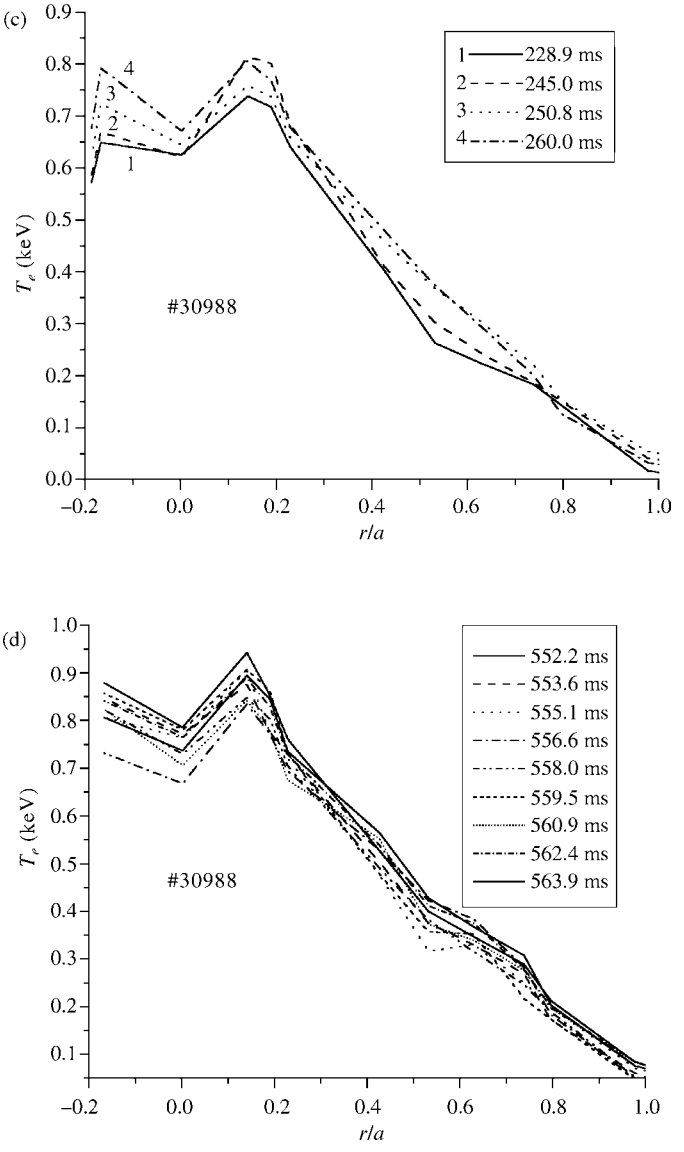


Figure 9. Continued.

becomes a deep hollow until a time of 250 ms, as shown in Fig. 9(b). Then, the initial peak profile seldom appears and the centroid of the temperature profile fully shifts to near the geometric centre, which can be clearly seen from Figs 9(c)–(e). The large variation of the horizontal displacement $\Delta_{\parallel}$ of the plasma is perhaps responsible for the centroid shift of the temperature profile $T_e(r)$. At the end of the high ramp-up phase at 259 ms, the temperature $T_e(-0.17a)$ reaches a similar value of $T_e(0.14a)$. After a time of 250 ms, the central hollow temperature profile is maintained until the end of the discharge independent of the rise rate of the plasma current and the sawtooth type, as exhibited in Figs 9(c) and (d). The same level strength of the sawtooth collapse during the high rate phase has a larger influence on the central

https://doi.org/10.1017/S0022377803002150 Published online by Cambridge University Press

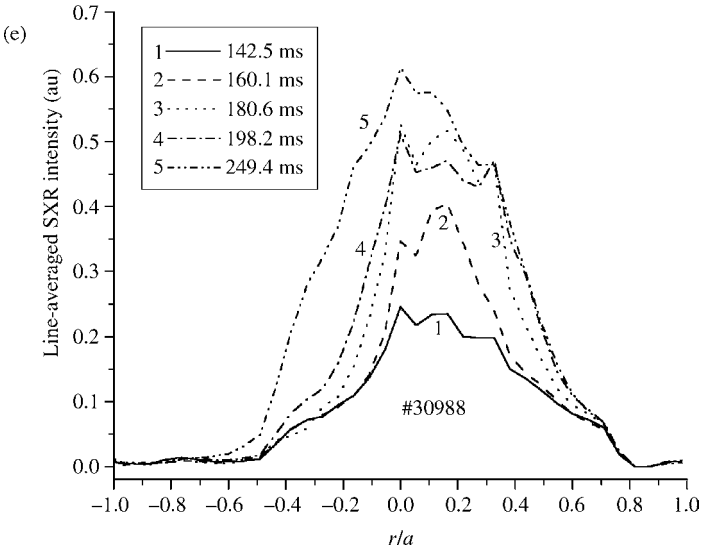


Figure 9. Continued.

temperature than that during the low rate phase due to the different temperature shape. The first double-sawtooth activities of type 1 and type 2 appear at 319.6 and 455 ms, respectively, both after the ramp-up phase of the plasma current, nearly 100 and 235 ms later after the formation of the central hollow profile $T_e(r)$. This means that the central hollow profile $T_e(r)$ is only a necessary but not sufficient condition for the occurrence of the double sawtooth – the skin effect probably does not produce a non-monotonic q profile during the current ramp-up phase.

According to some proposed theoretical models [7, 22, 23], double-sawtooth oscillations are associated with a double-tearing reconnection mode in a reversed magnetic shear plasma, which requires a hollow current profile. Other than by direct measurement of a plasma current profile, we could not obtain direct evidence to conclude whether the events are associated with a double-tearing reconnection mode. However, according to Kadomtsev's tearing model, the existence of the double-sawtooth activity indicates the formation of magnetic islands with two $q = 1$ surfaces. The second magnetic reconnection causes the larger central collapse and encompasses the magnetic axis, which is similar to that seen in a single sawtooth, whereas the first reconnection does not extend to the magnetic axis and is outside of the partial collapse. The hollow $T_e(r)$ profile may be attributed to increasing the electron thermal diffusivity due to the skin effect during the ramp-up phase of the plasma current. This probably causes the formation of a hollow current density profile. It suggests that variations of electron temperature profile may change the MHD behaviour and the current density profile. Because small and double sawteeth usually occur together, this suggests that a small or localized change of the plasma parameters may affect the characteristics of the sawtooth significantly. The occurrence and evolution of the first collapse of the double sawtooth, and its influence on the following full collapse probably depends on the local parameters, especially on the local q value and its shear. Owing to the limitation of the given spatial and time resolution (~3 cm, 1.5 ms) for the ECE radiometer measurement, it is difficult to analyse fine variations of the temperature among

https://doi.org/10.1017/S0022377803002150 Published online by Cambridge University Press

the two first collapses and the two second collapses of the double sawtooth, and the single sawtooth collapse.

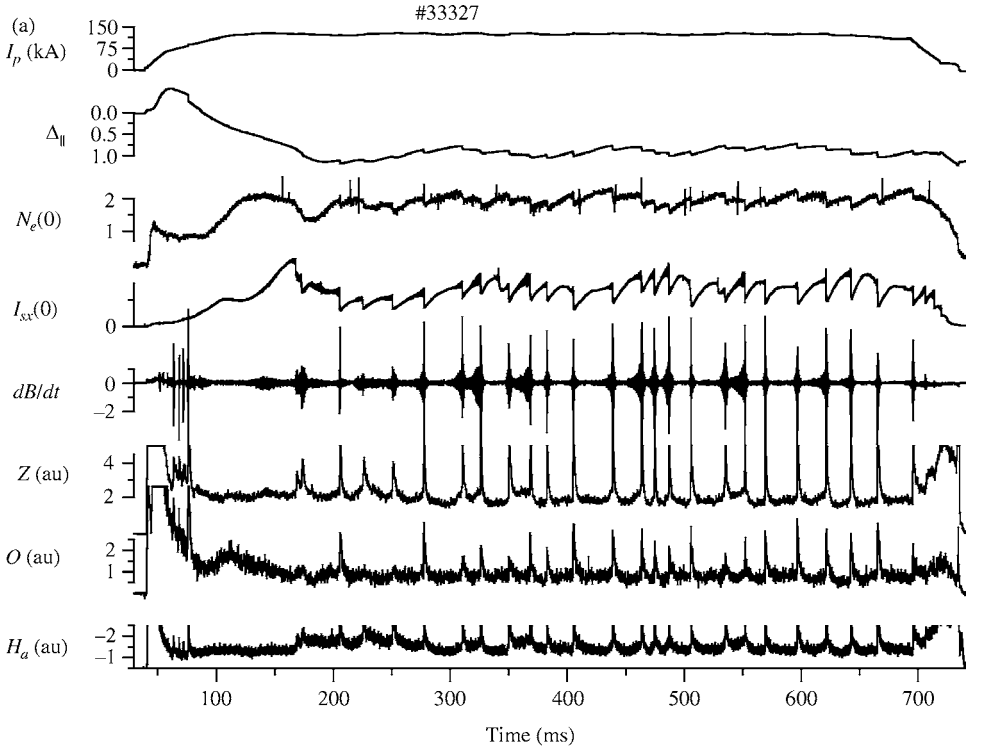
5. Monster sawtooth activities in an ohmically heated plasma

Sometimes in some cases of an HT-7 ohmic plasma, such as the safety factor q_a between 4.2 and 4.7, $\bar{N}_e(0) = 1.5\text{–}2.5 \times 10^{13}\,\mathrm{cm}^{-3}$ and $Z_{\mathrm{eff}} = 3.0\text{–}6.0$, monster sawtooth oscillations emerge without apparent deterioration of confinement and without major plasma disruption. They are characterized by a series of large core collapses belonging to global fluctuations on SXR intensity traces with a long period ($T_s \leqslant 33.5\,\mathrm{ms}$, several times that of the particle confinement τ_P), a large-amplitude fluctuation ($\Delta I_{sx}/\bar{I}_{sx} \leqslant 76\%$) and a large inversion radius ($r_s \leqslant 0.4a$). It is thought to normally be associated with the presence of fast particles in the plasma, which could be initiated for many reasons such as a moderate or high impurity distribution, an electron density fluctuation or a dissipation of energetic electrons induced by a small internal disruption, etc.

Figure 10(a) illustrates one event of the monster sawtooth oscillation activity induced by an off-axis peaking distribution of the electron density $N_e(r)$. Lots of ELM-like bursts are observed apparently on visible bremsstrahlung Z, H_α optical radiation, XUV bolometer and oxygen line emission, and weak bursts on carbon line emission are also found therein. These bursts correspond to the negative SXR sawteeth outside of the $q = 1$ surface and are more intense on the edge region than that on the central region especially on the low field side, but with an obvious time delay representing the period of a perturbation travelling from the $q = 1$ region to the plasma boundary. Corresponding to each core collapse, the central electron density decreases with relative perturbations $\Delta N_e/N_e \leqslant 9\%$, the horizontal displacement $\Delta_\parallel$ shifts inward from the outside position just before the occurrence of the collapse and the loop voltage changes with positive or negative spikes, as shown in Fig. 10(b). No relative bursts of hard x-ray radiation suggest no apparent generation of energetic electrons. Although core sawtooth collapses enhance the loss of energy and particles from the core plasma and also enhance wall recycling, the plasma has been sustained only with small current fluctuations $\Delta I_P/\bar{I}_P \leqslant 5\%$ and without apparent deterioration of the confinement and without major disruption. The evolution of the electron temperature $T_e(r)$ profile given in Fig. 11 shows the global decrease during the major and giant sawtooth collapses, and the corresponding evolution of the SXR intensity I_{sx} profiles is of a generally similar variation since macroscopic parameters of the plasma have relative fluctuations during core collapses as well.

For some core collapses with longer periods, complex behaviours are exhibited on the SXR intensity signals. A compound sawtooth with one or more (up to five) partial collapses is frequently observed. Nearly all single sawteeth and compound sawteeth have precursory or successor oscillations of an $m = 1$ MHD activity with a frequency of 4–9 kHz, sometimes a coupling of $m = 1$ and 2 activities appears on the precursory oscillation. The $m = 2$ oscillations have a phase inversion at radii of $0.22a$ and $0.55a$ for the LFS and that of $-0.11a$ and $-0.49a$ for the HFS. A double-frequency oscillation can also be seen near the region of the $q = 2$ surface. Sometimes the partial collapse is very localized, only a very small redistribution of energy around the $q = 1$ surface can be seen. In contrast to full collapses, during partial collapses, only weak bursts are observed on the XUV bolometer – no influence on the outward shift of the horizontal displacement $\Delta_\parallel$, on the loop voltage

https://doi.org/10.1017/S0022377803002150 Published online by Cambridge University Press



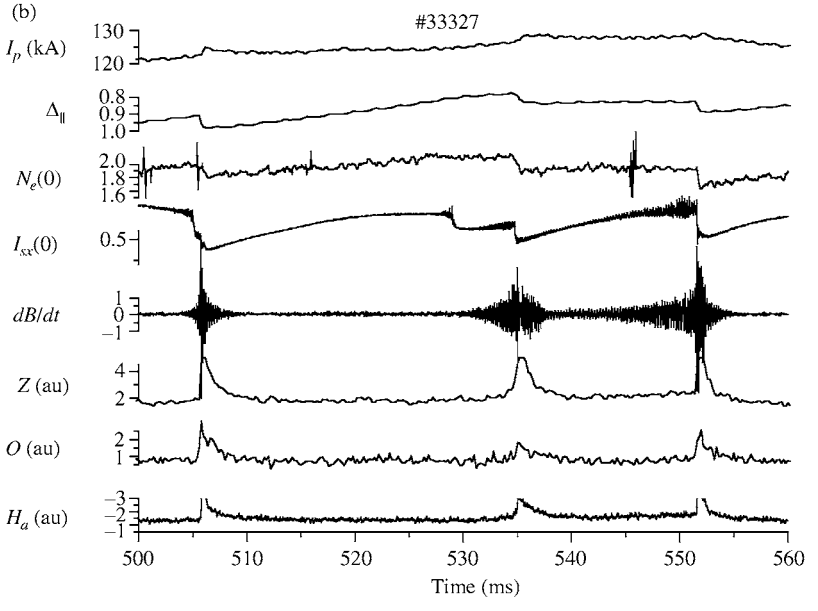


Figure 10. (a) Plasma performance on several diagnostic signals for the typical ohmic shot 33327 with the monster sawtooth oscillation initiated by the off-axis peaking distribution of the electron density $\bar{N}_e(r)$ ($I_p = 130.9\,\mathrm{kA}/0.7\,\mathrm{s}$, $\bar{N}_e(0) = 1.5\text{–}2.5 \times 10^{13}\,\mathrm{cm}^{-3}$, $Z_{\mathrm{eff}} = 3\text{–}6$ and $q_a = 4.2\text{–}4.7$). (b) The expanded traces of several diagnostic signals during the monster sawtooth oscillation corresponding to Fig. 10(a).

https://doi.org/10.1017/S0022377803002150 Published online by Cambridge University Press

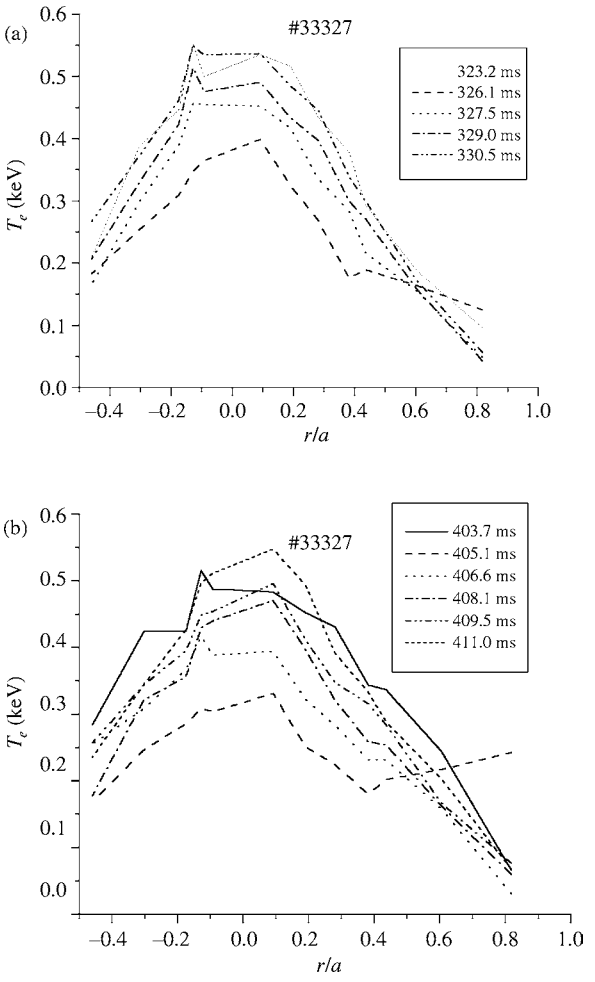


Figure 11. Temporal evolution of the electron temperature profile $T_e(r)$ during the monster sawtooth oscillation for the ohmic shot 33327. (a) Before, during and after a major sawtooth collapse at $t = 325.8$ ms, (b) before, during and after a giant sawtooth collapse at $t = 405$ ms.

and on the plasma current have been found, and the plasma continues the recovery trends from the previous full core collapse, which are accompanied with an improved particle confinement and density profile peak.

Abundant MHD phenomena are observed on the SXR intensity signal during the period of the monster sawtooth activity and in most cases fully correlated to MHD fluctuations on magnetic pickup probes, as shown in Fig. 12. They are identified with a mode growing before full collapse (a), suppression (a) and saturation (b) after full collapses, mode generation after the partial collapse (c) and after the full collapse (d), without mode generation during the partial (a and d) and during the full collapse (d). It can be seen that whether partial collapses initiate mode oscillation is not the key factor for the coming full collapse, the successor mode activity is dependent on the strength of partial collapses and may affect the strength of the full collapse. Herein, fine evolutions of electron temperature $T_e(r)$ during the partial

https://doi.org/10.1017/S0022377803002150 Published online by Cambridge University Press

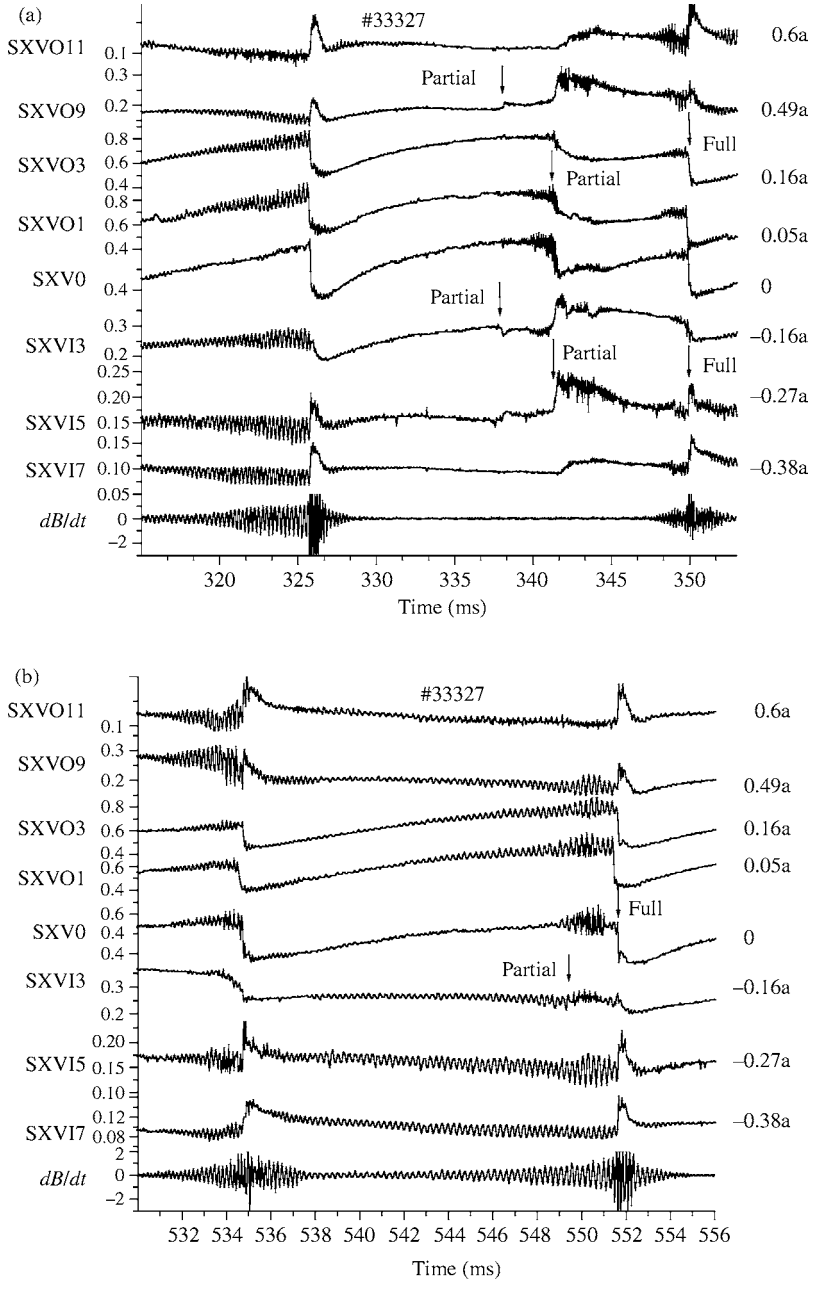
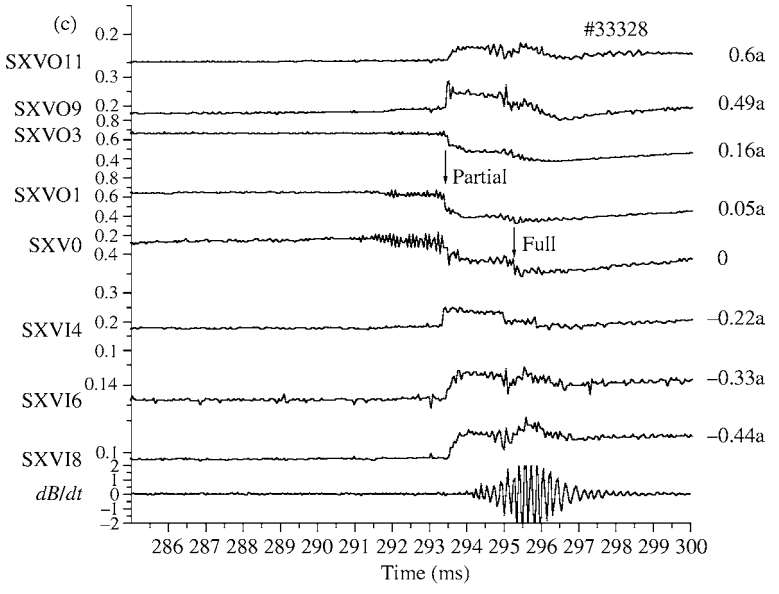


Figure 12. Abundant MHD oscillations during the monster sawtooth collapse on the signals of SXR intensity and magnetic pickup probes for typical shots 33327 and 33328. Mode growing before full collapses (a), suppression (a) and saturation (b) after full collapses, mode generation after the partial collapse (c) and after the full collapse (d), without mode generation during the partial (a and d) and during the full collapse (d).

https://doi.org/10.1017/S0022377803002150 Published online by Cambridge University Press



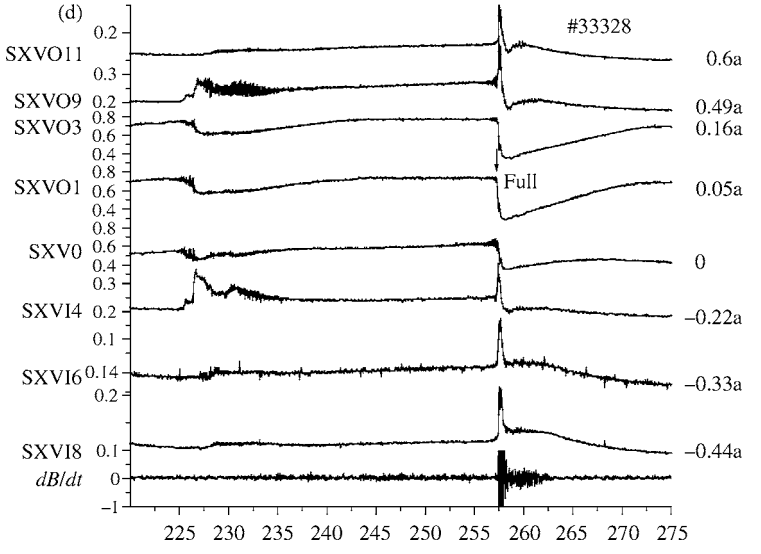


Figure 12. Continued.

collapse are difficult to identify due to the given low time and spatial resolution of the ECE radiometer measurement.

6. Summary

The sawtooth activity in an ohmically heated HT-7 plasma has been studied carefully and summarized using the soft x-ray diagnostic, magnetic pickup probes and other diagnostics. General behaviours of the sawtooth instability: the period, the

https://doi.org/10.1017/S0022377803002150 Published online by Cambridge University Press

amplitude, rising and dropping speeds, precursor and successor with $m/n = 1/1$ oscillations overlapped on the sawtooth and the inversion radius r_s, are correlated to plasma conditions such as the electron density N_e and the temperature T_e, the impurity content and the plasma edge parameters. As $\bar{N}_e$ increases, generally speaking, the sawtooth activity may become strong with a longer period T_s, a larger relative amplitude fluctuation $\Delta I_{sx}/\bar{I}_{sx}$, a wider region of sawtooth fluctuations and a larger radius r_s, and evolves from a small to a moderate sawtooth, to a major or even a giant sawtooth (r_s from normal $0.15a$ to $0.3a$). The shortest period of sawtooth collapse is around 25–30 μs. Experimental properties of the two types of double sawtooth and monster sawtooth activities are also studied. The existence of the double-sawtooth activity is correlated tightly with the central hollow temperature profile and indicates the formation of magnetic islands with two $q = 1$ surfaces, which is consistent with the Parail–Pereverzev tearing model. The hollow temperature profile is attributed to increasing the electron thermal diffusivity due to the skin effect during the ramp-up phase of the plasma current. This probably causes the formation of a hollow current density profile. The occurrence of the double sawtooth, and the influence of the first collapse on the following second collapse probably depends on the local plasma parameters, especially on the local q value and its shear. It suggests that variations of the electron temperature profile may change the MHD behaviour and the current density profile. In some cases such as the safety factor q_a between 4.2 and 4.7, $\bar{N}_e(0) = 1.5\text{–}2.5 \times 10^{13}\,\mathrm{cm}^{-3}$ and $Z_{\mathrm{eff}} = 3.0\text{–}6.0$, monster sawtooth activity with a long period ($T_s \leqslant 33.5$ ms), significantly large amplitude fluctuation ($\Delta I_{sx}/\bar{I}_{sx} \leqslant 76\%$) and large reversal radius ($r_s \leqslant 0.4a$) often emerges without apparent deterioration of the plasma confinement and without major plasma disruption. During the events, abundant MHD phenomena including the long partial sawtooth collapses are exhibited.

Acknowledgements

The authors are grateful to all members of the HT-7 group for their contributions to the HT-7 experiments. They also want to express their special acknowledgements to Dr Shouying Zhang, Dr Bolong Ding and Mr Li Zeng for their help in processing the experimental data. The HT-7 experimental project is supported by the Chinese Nature Science Funds under contract number 10235010.

References

[1] Von Goeler, S., Stodiek, W. and Sauthoff, N. 1974 *Phys. Rev. Lett.* **33**, 1201.
[2] Alper, B. et al. 1997 *Rev. Sci. Instrum.* **68**, 778.
[3] Da Cruz, D. F. Jr. and Donné, A. J. H. 1994 *Rev. Sci. Instrum.* **65**, 2295.
[4] Anton, M. et al. 1996 *Plasma Phys. Control. Fusion* **38**, 1849.
[5] Bussac, M. N. et al. 1975 *Phys. Rev. Lett.* **35**, 24.
[6] Wesson, J. A. 1986 *Plasma Phys. Control. Fusion* **28(1A)**, 243.
[7] Kadomtsev, B. B. 1975 *Sov. J. Plasma Phys.* **1**, 389.
[8] Wesson, J. A. 1990 *Nucl. Fusion* **30**, 2545.
[9] Gimblett, C. G. and Hastie, R. J. 1994 *Plasma Phys. Control. Fusion* **36**, 1439.
[10] Haas, F. A. and Thyagaraja, A. 1995 *Plasma Phys. Control. Fusion* **37**, 415.
[11] Campbell, D. J. et al. 1986 *Nucl. Fusion* **26**, 1085.

https://doi.org/10.1017/S0022377803002150 Published online by Cambridge University Press

[12] Campbell, D. J. et al. 1987 *Proc. 12th IAEA Conf. on Plasma Phys. and Control. Nucl. Fusion Res.*, Nice, France, IAEA, Vienna, Vol. 2, 433.

[13] Xie, J. K. et al. 1996 *Proc. 16th IAEA Conf. Fusion Energy*, Montreal, Canada, IAEA, Vienna, Vol. 1, 685. IAEA-CN-64/AP1-13.

[14] Yuanxi, Wan et al. 2000 *Nucl. Fusion* **40**, 1057.

[15] Zhang, S. Y. et al. 2000 *Plasma Phys. Control. Fusion* **42**, 743.

[16] Liqun, H. et al. 2000 *Plasma Sci. Technol.* **2**, 515.

[17] Qingchu, Zh., Lei, Ch. and HT-7 group 1997 *Proc. 11th Int. Stellarator Conf. and the 8th Int. Toki Conf.* (*ITC-8*).

[18] Fredrickson, E. D. et al. 1986 *Nucl. Fusion* **26**, 849.

[19] Jiangang, L. et al. 1999 *Nucl. Fusion* **39**, 973.

[20] Pfeiffer, W. 1985 *Nucl. Fusion* **25**, 673.

[21] Campbell, D. J. et al. 1986 *Nucl. Fusion* **26**, 1085.

[22] Strait, E. J. et al. 1995 *Phys. Rev. Lett.* **75**, 4421.

[23] Chang, Z. et al. 1996 *Phys. Rev. Lett.* **77**, 3553.

https://doi.org/10.1017/S0022377803002150 Published online by Cambridge University Press